

## Supporting Information

### **Efficacious engineering on charge extraction for realizing high-efficient perovskite solar cells**

*Shizhong Yue, Kong Liu, Xu Rui, Meicheng Li, Muhammad Azam, Kuankuan Ren, Jun Liu,  
Yang Sun, Zhijie Wang\*, Shengchun Qu\*, Dawei Cao, Xiaohong Yan, Yong lei\* and Zhanguo  
Wang*

## Section 1. Discussion on the Cl incorporation to the perovskite structure

In comparison with the  $\text{CH}_3\text{NH}_3\text{PbI}_3$  film,  $\text{PbI}_2$  is not observable, indicating that the precursor,  $\text{PbI}_2$ , has been consumed in the current ratio (shown in Figure 1c). However, when we reduce the usage of 10%  $\text{PbI}_2$  and use the same molar ratio of  $\text{PbCl}_2$  instead (the precursor ratio for  $\text{CH}_3\text{NH}_3\text{PbI}_3$  is 1 ( $\text{CH}_3\text{NH}_3\text{I}$ ): 1 ( $\text{PbI}_2$ ) and that for  $\text{CH}_3\text{NH}_3\text{PbI}_{3-x}\text{Cl}_x$  is 1( $\text{CH}_3\text{NH}_3\text{I}$ ): 0.9 ( $\text{PbI}_2$ ): 0.1 ( $\text{PbCl}_2$ )), the resulting film does not show the presence of  $\text{PbCl}_2$ , but the  $\text{PbI}_2$ . Due to the different ionic nature of  $\text{PbI}_2$  and  $\text{PbCl}_2$ ,  $\text{PbCl}_2$  could be superior to react with  $\text{CH}_3\text{NH}_3\text{I}$  over  $\text{PbI}_2$ . The overall reaction could be described by the following equations:<sup>1</sup>



First,  $\text{PbCl}_2$  reacts with  $\text{CH}_3\text{NH}_3\text{I}$  and generates  $\text{CH}_3\text{NH}_3\text{PbI}_3$  and  $2\text{CH}_3\text{NH}_3\text{Cl (g)}$ , then these two products will reaction with  $\text{PbI}_2$  and  $\text{CH}_3\text{NH}_3\text{I}$  and generate the production  $\text{CH}_3\text{NH}_3\text{PbI}_{3-x}\text{Cl}_x$ . During the annealing process, the gas phase of excess of  $\text{CH}_3\text{NH}_3\text{Cl}$  will be released from the film and we could observe that Cl content is decreased from the surface to the bulk of the film until to a stable value (Figure S1b). Not only from XPS measurement, the presence of  $\text{CH}_3\text{NH}_3\text{PbI}_{3-x}\text{Cl}_x$  could be proven by the widened band gap and shifted band gap position in comparison with  $\text{CH}_3\text{NH}_3\text{PbI}_3$ . To give a more direct evidence, we detached the grains from the film and carried out TEM measurement. As shown in Figure S2, the grains exhibit a nice crystallinity and the EDS mapping for the grain shows that Cl distributed homogenously in the grains, indicative of that Cl indeed exists in the crystals. According to the calculation by Mosconi et al., Cl atoms preferentially occupy the apical positions in the  $\text{PbI}_4\text{X}_2$  octahedra in the perovskite structure.<sup>2</sup> Due to the fact that  $\text{PbCl}_2$  is consumed and  $\text{PbI}_2$  is left, it is also possible that the small amount of Cl element could locate in the place which belongs to I element but the main I sites are still taken up by I element.

## Section 2. The advantage of the FTO substrates

First, the used FTO substrate has sheet resistance of  $8.5 \Omega/\square$  (from NSG Group TEC-A7). This value is even lower than the value from ITO glass ( $8.5$  vs  $12.85 \Omega/\square$ ) and much lower than that from the conventional FTO substrate. Second, the used FTO shows a higher thermal stability than ITO glass. After annealed at  $340^\circ\text{C}$  for 1h, the resistance of the used FTO glass only shows

a slight increase from 8.5 to 10.3  $\Omega/\square$ , while ITO glass present a sharp increase in resistance from 12.8 to 53.4 $\Omega/\square$ . Third, the transmittance of the used FTO substrate exhibit a higher tolerance against high temperature than that from the ITO glass.

### **Section 3. The impedance analysis of the device**

All the impedance spectra in this work are fitted by the equivalent circuit in the corresponding figures.  $R_s$  stands for the series resistance of the system, including the internal resistance of the electrodes.  $R_1$  and  $R_2$  stand for the interface resistance (e.g., the recombination resistance and contact resistance at the interfaces) at the  $\text{NiO}_x/\text{perovskite}$  or  $\text{perovskite}/\text{PC}_{61}\text{BM}$ .  $R_1$  and  $R_2$  are related to the high-frequency semicircle and low-frequency semicircle, respectively. This definition is in agreement with the references.<sup>3</sup> In Figure 2f, the presence of the suitable thickness of the ZrAcac results in the decrease in  $R_s$ ,  $R_1$  and  $R_2$ , in comparison with the reference device and the device with ethanol treatment. The improvement in electron transport at the interface of  $\text{PC}_{61}\text{BM}$  and Al has a dramatically positive impact on  $R_1$  and  $R_2$  while  $R_s$  only shows a slight decrease. This is consistent with the definition that  $R_1$  and  $R_2$  are related to the interface charge transport. With regard to the device performance, the reduction in the resistances ( $R_1$ ,  $R_2$  and  $R_s$ ) usually indicates a low possibility of charge recombination and thus a remarkable enhancement in FF. Too much loading of ZrAcac at the interface would deteriorate the electron transport at the interface. The two interface-related resistances,  $R_1$  and  $R_2$ , both show a significant increase ( $R_1$ : more than 10 folds;  $R_2$ : more than 100 folds).  $R_s$  only shows a slight variation (less than 10%). FF would be decreased accordingly. In Figure S16, the purpose of Cu doping (e.g., 5%) is tuning the band gap alignment and make it favorable for hole transport at the interface. Thus,  $R_1$  and  $R_2$  both show a remarkable decrease for the device with 5% Cu doped  $\text{NiO}_x$  in comparison with the counterparts whose bandgap alignment is not optimized, like the device with intrinsic  $\text{NiO}_x$  and the one with 20% Cu doped  $\text{NiO}_x$ . This is mainly responsible for the large FF of the optimized device. In Figure 5c, the high conductivity of the used FTO substrate is directly related to the internal charge transport of the electrode and thus  $R_s$  of the FTO involved device is much lower than the ITO involved device. The improvement in conductivity of the FTO electrode would be also helpful for reducing the charge aggregation at the interface and the charge recombination efficiency would be decreased accordingly. This could be indicated from the reduction in  $R_1$  and  $R_2$ . The decrease in all the

three kinds of resistances is directly related to the high FF of the FTO based device.

#### Section 4. The supporting figures

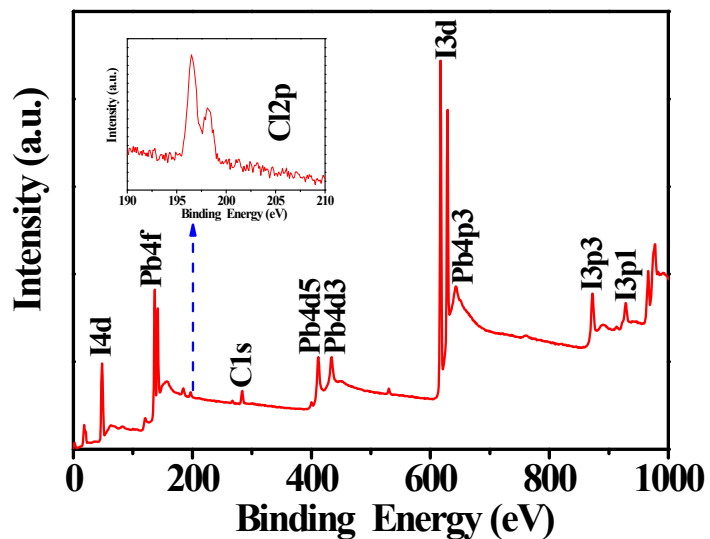
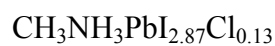


Figure S1a The X-ray photoelectron spectrum of  $\text{CH}_3\text{NH}_3\text{PbI}_{3-x}\text{Cl}_x$  film, the inset is the XPS spectrum of Cl element.

Name	Peak BE	Height Counts	FWHM eV	Area (P) CPS.eV	Atomic %
Pb4f	136.71	72136.5	0.96	298671.91	24.97
Cl2p	196.54	6011.43	1.02	9091.31	9.44
I3d	617.23	175401	1.14	844822.64	65.59

From the XPS elemental analysis, the stoichiometry of this film is approximately equal to



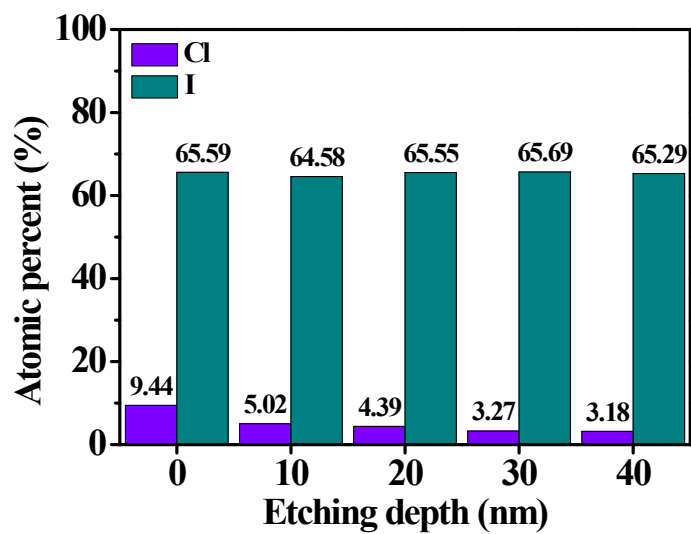


Figure S1b The variation of atomic percent with different etching depth (0 nm means the surface of perovskite film).

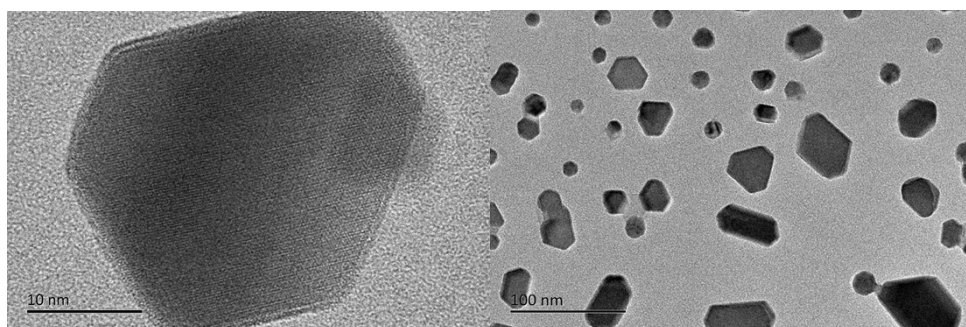


Figure S2a The HRTEM images of the perovskite film.

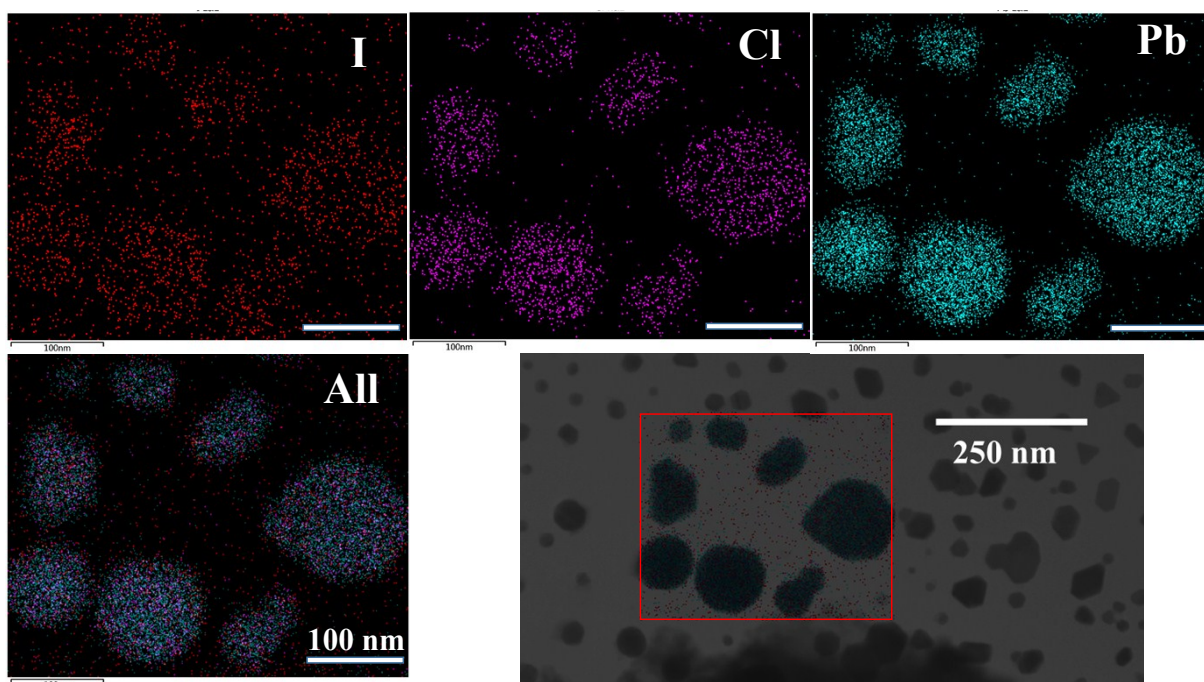


Figure S2b The EDS mapping for the grains, the scale bar is 100 nm. All the mapping images were obtained from the square in the STEM image (bottom right).

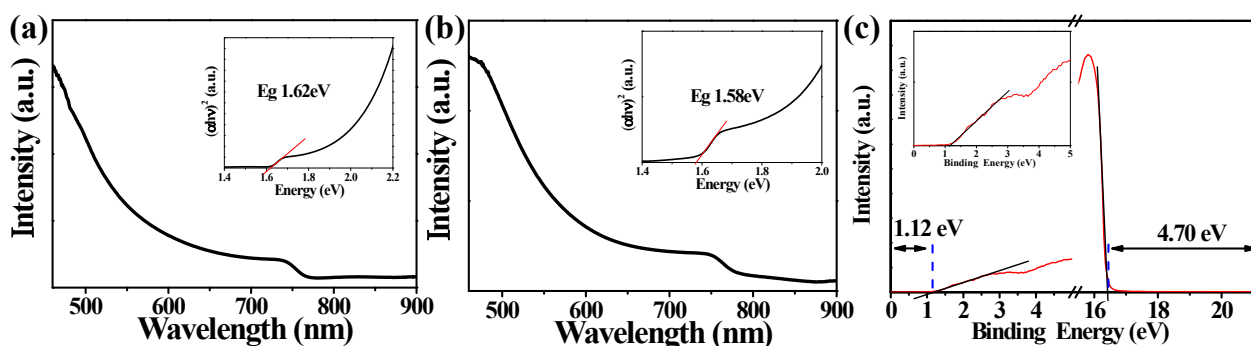


Figure S3 Absorbance spectrum of (a)  $\text{CH}_3\text{NH}_3\text{PbI}_{3-x}\text{Cl}_x$  and (b)  $\text{CH}_3\text{NH}_3\text{PbI}_3$  film on ITO substrates, inset shows the corresponding Tauc plots. (c) The ultraviolet photoelectron spectrum of the  $\text{CH}_3\text{NH}_3\text{PbI}_{3-x}\text{Cl}_x$ . The inset zooms in the low binding energy region.

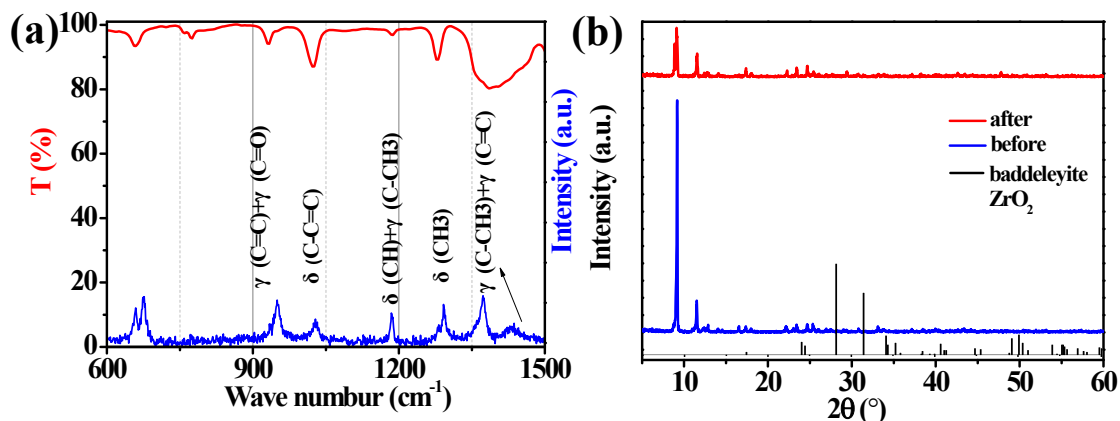


Figure S4 (a) The Fourier infrared (up) and Raman (down) spectra of the ZrAcac. (b) The XRD patterns of the ZrAcac powders, the original powder (dark line) and the powder got by evaporating the ethanol in ZrAcac solution (red line). The measured XRD patterns for ZrAcac are in good agreement with the reported result.<sup>4</sup>

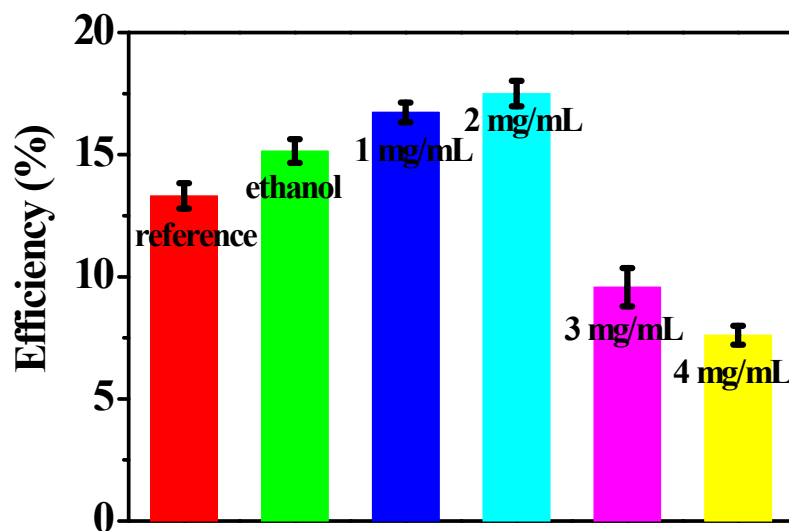


Figure S5 The corresponding statistical values of PCE in figure 2b.

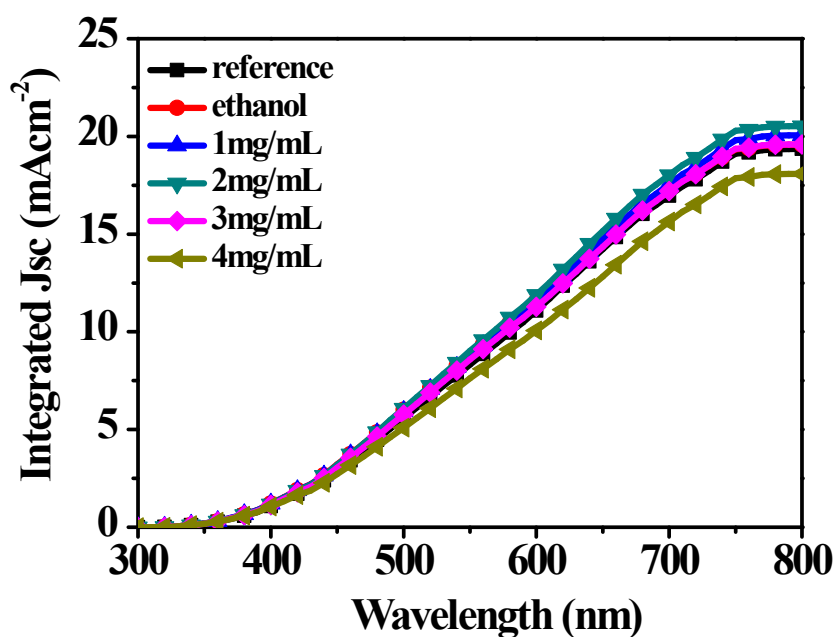


Figure S6 The corresponding integrated  $J_{sc}$  of the devices in figure 2c.

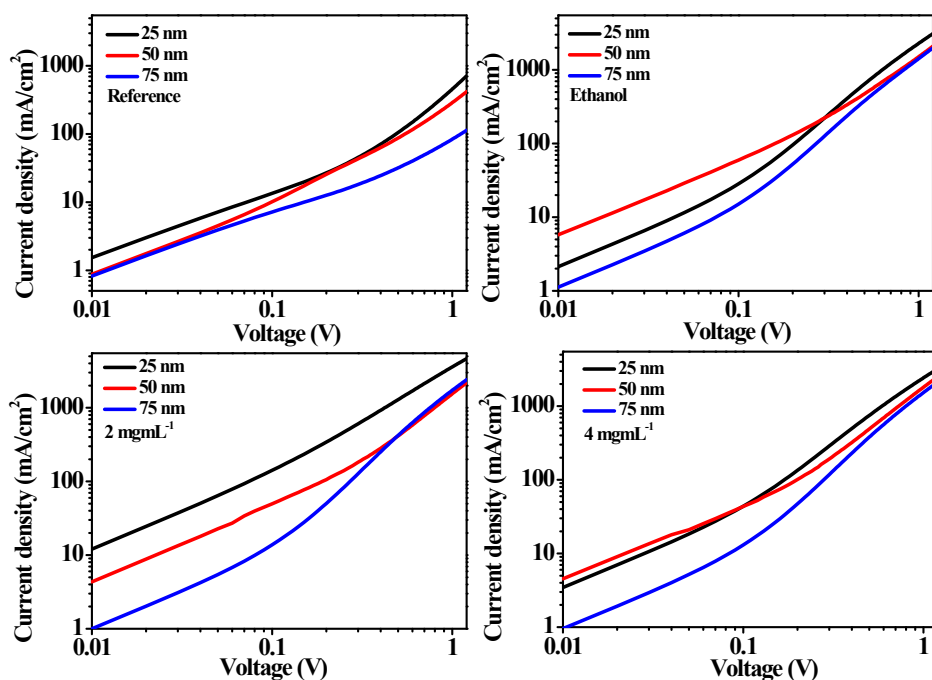


Figure S7a The experimental current density-applied voltage (J-V) characteristics of electron-only devices with active layer of 25 nm, 50 nm and 75 nm.

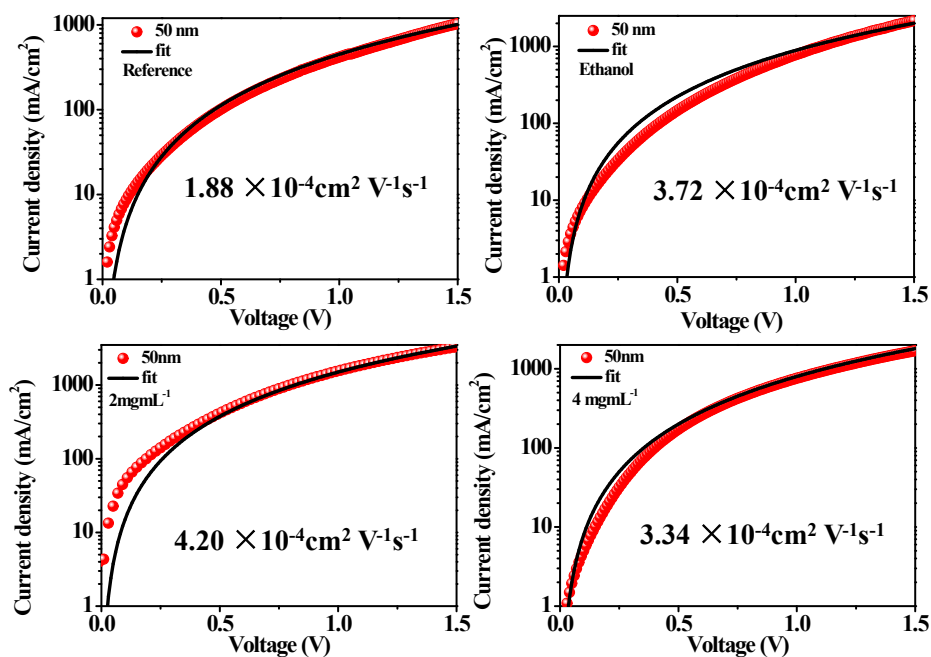


Figure S7b The fitting results to Fig. S7a as the SCLC model

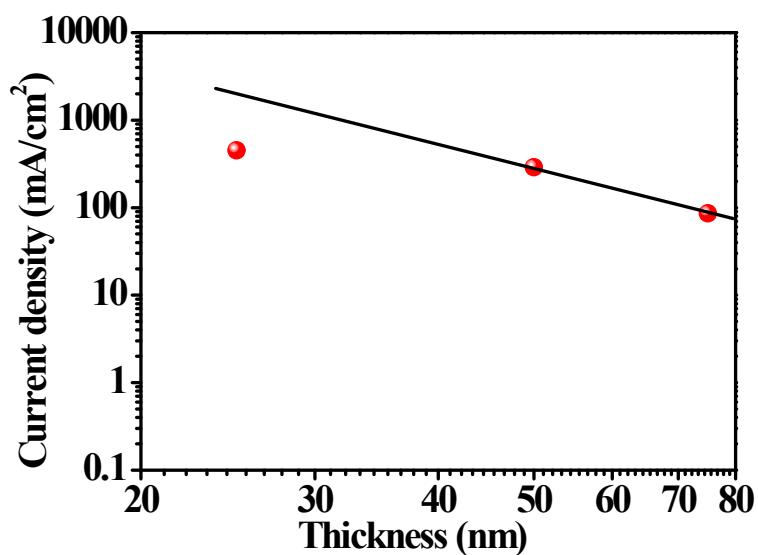


Figure S7c The log-log plot of thickness dependence of current density at a fixed bias of 1 V (ITO/Al/PCBM/Al). The red dots are experimental data and the solid line is fit according to the relation  $J \propto V^2/L^3$ , where  $L$  is the thickness of the PC<sub>61</sub>BM.

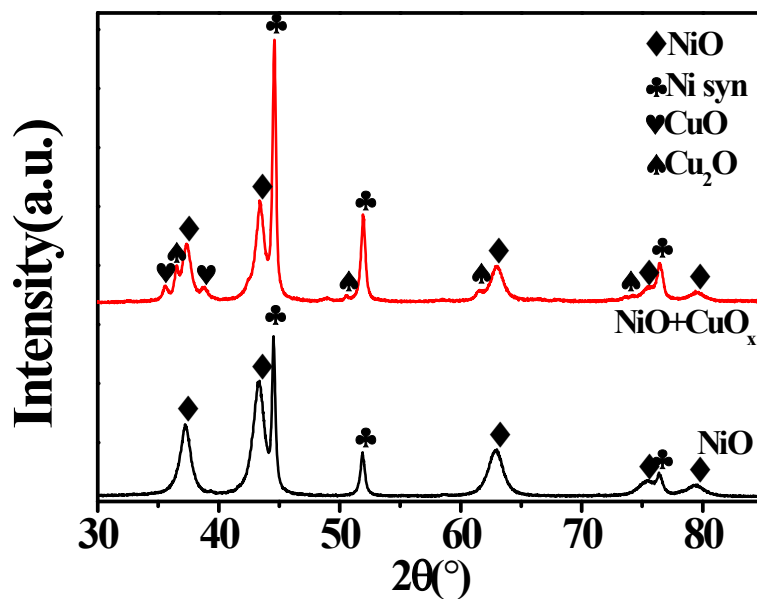


Figure S8 X-ray diffraction patterns of the  $\text{NiO}_x$  and 5% Cu doped  $\text{NiO}_x$  powder.

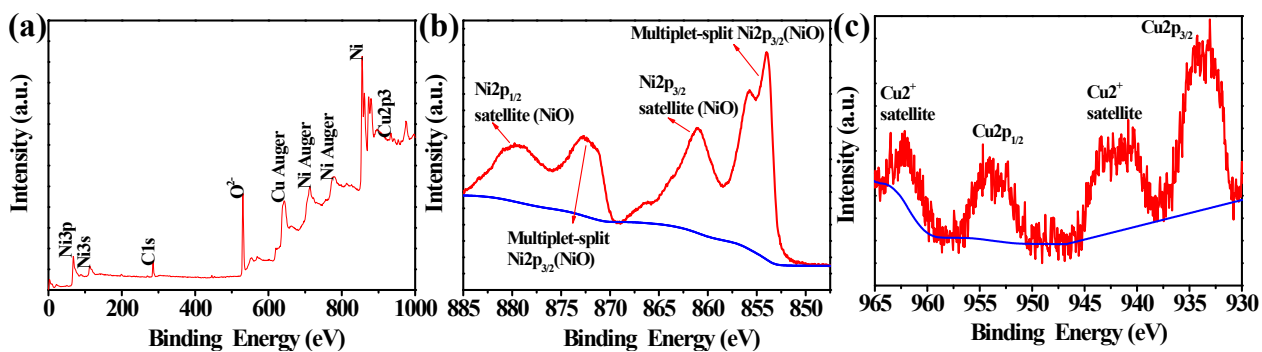


Figure S9 (a) The X-ray photoelectron spectrum of 5% Cu doped  $\text{NiO}_x$  film. (b) The XPS  $\text{Ni}2p$  core level spectrum in S9a. (c) The XPS  $\text{Cu}2p$  core level spectrum in S9a.

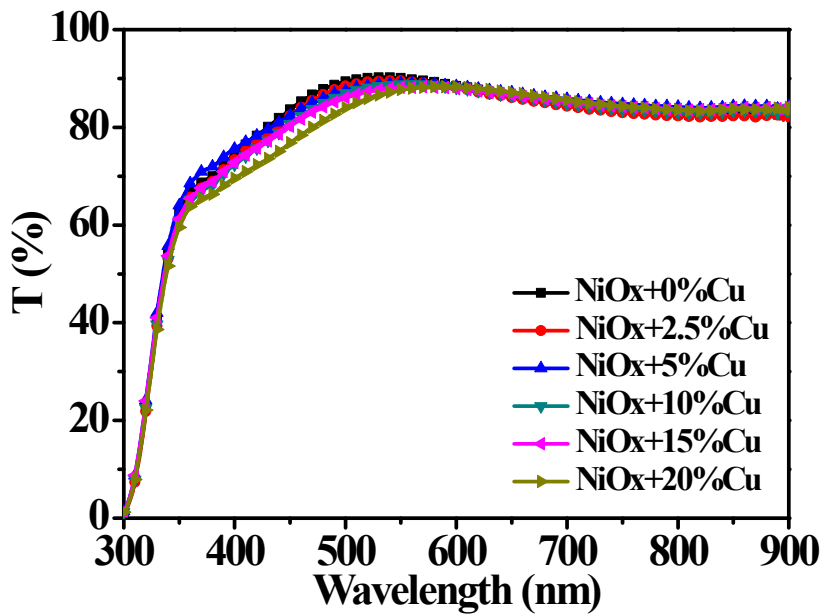


Figure S10 The transmission spectra of the series of NiO<sub>x</sub> films on ITO substrates.

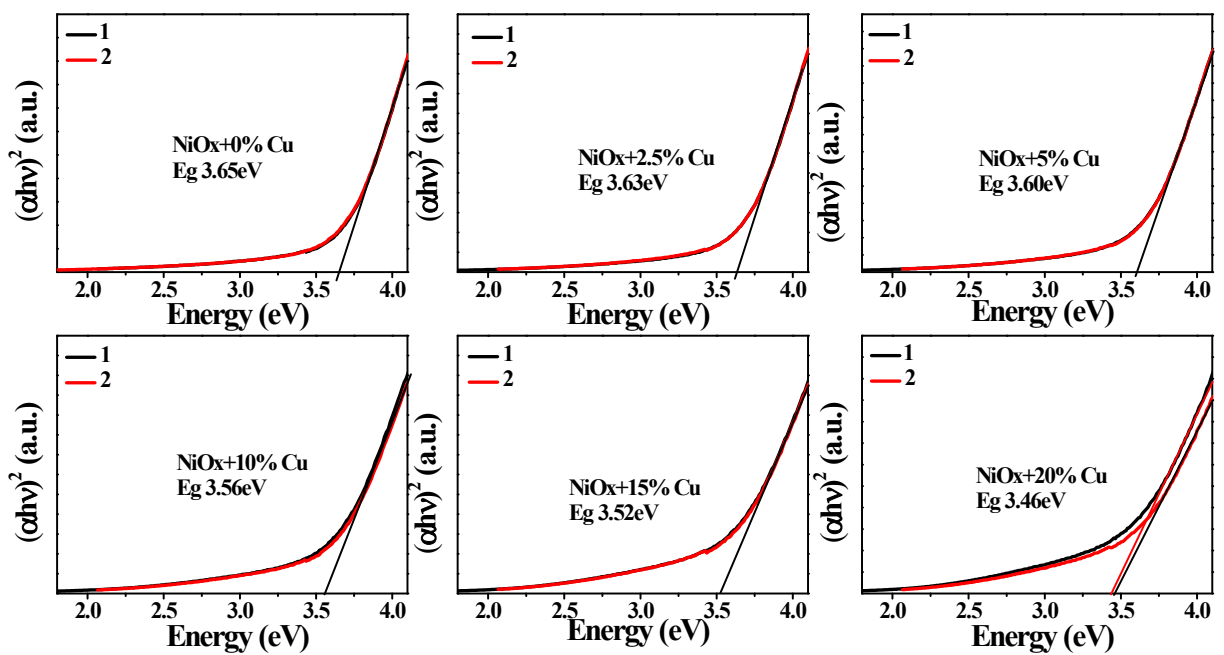


Figure S11 The Tauc plots of the doped NiO<sub>x</sub> films on quartz substrates, each condition with two samples.

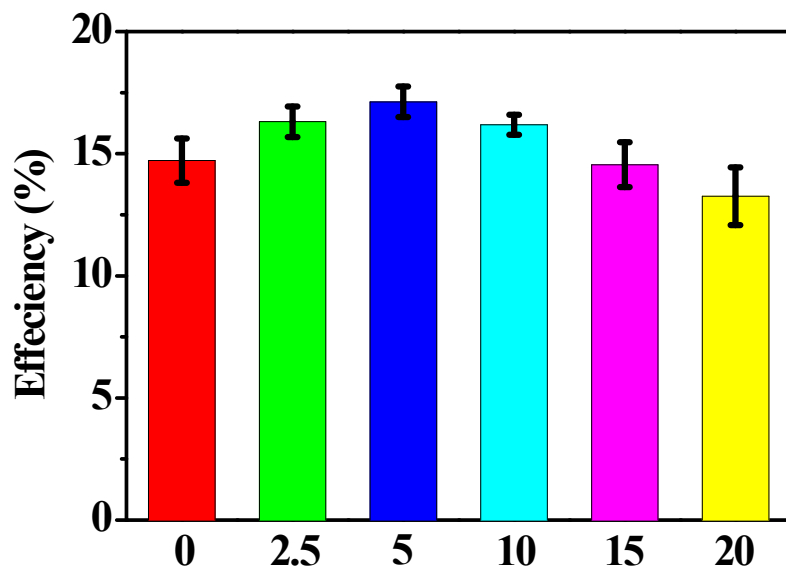


Figure S12 The corresponding statistical values of PCE in figure 3b.

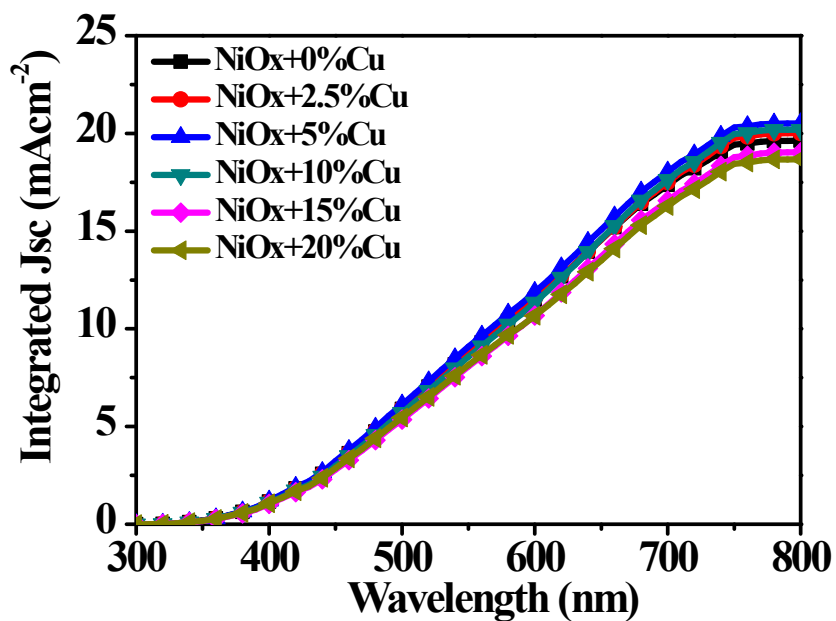


Figure S13 The corresponding integrated  $J_{sc}$  of the devices figure 3c.

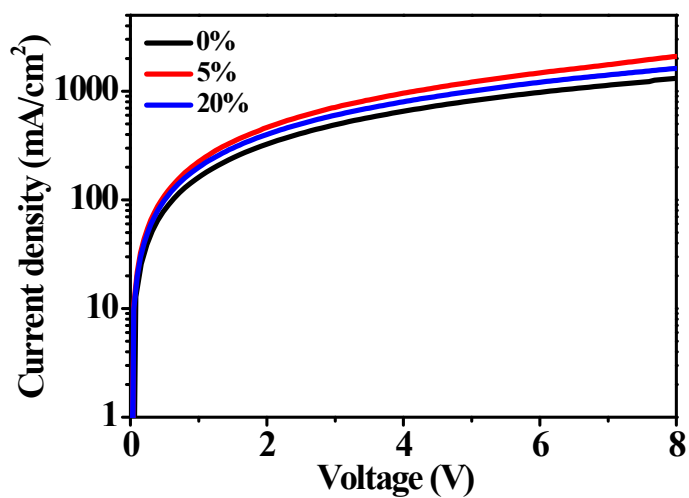


Figure S14 (a) J–V curves of the hole-only devices with the structure of ITO/NiO<sub>x</sub> (0, 5 and 20% of Cu doping, respectively)/CH<sub>3</sub>NH<sub>3</sub>PbI<sub>3-x</sub>Cl<sub>x</sub>/Au.

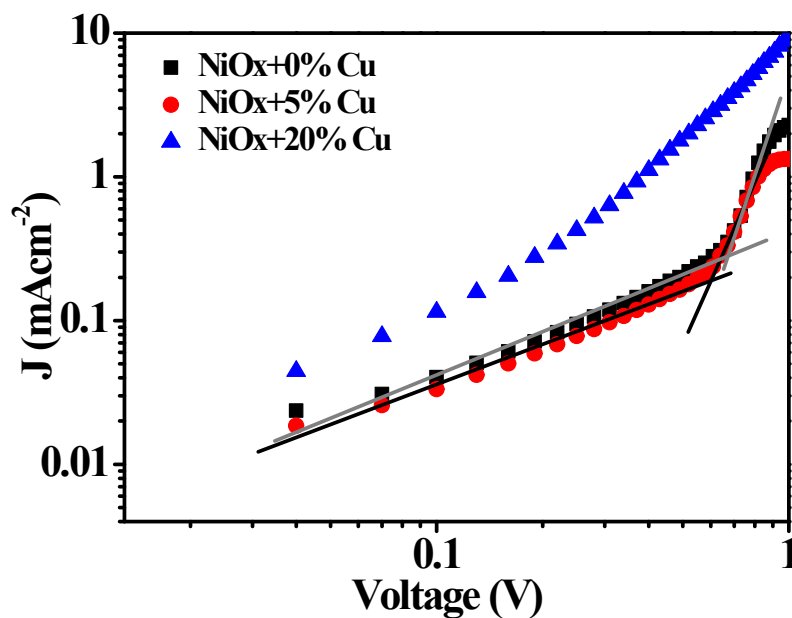


Figure S15 J–V curves of the hole-only devices with the structure of ITO/NiO<sub>x</sub> or Cu doped NiO<sub>x</sub>/CH<sub>3</sub>NH<sub>3</sub>PbI<sub>3-x</sub>Cl<sub>x</sub>/Au.

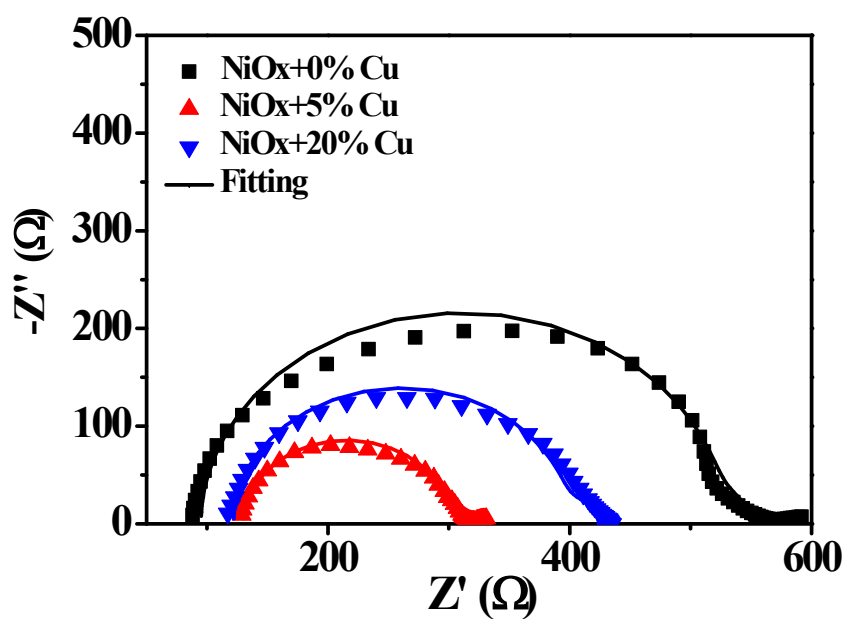


Figure S16 Nyquist plots of the devices with Cu doped NiO<sub>x</sub> measured in dark at  $V \approx V_{oc}$ .

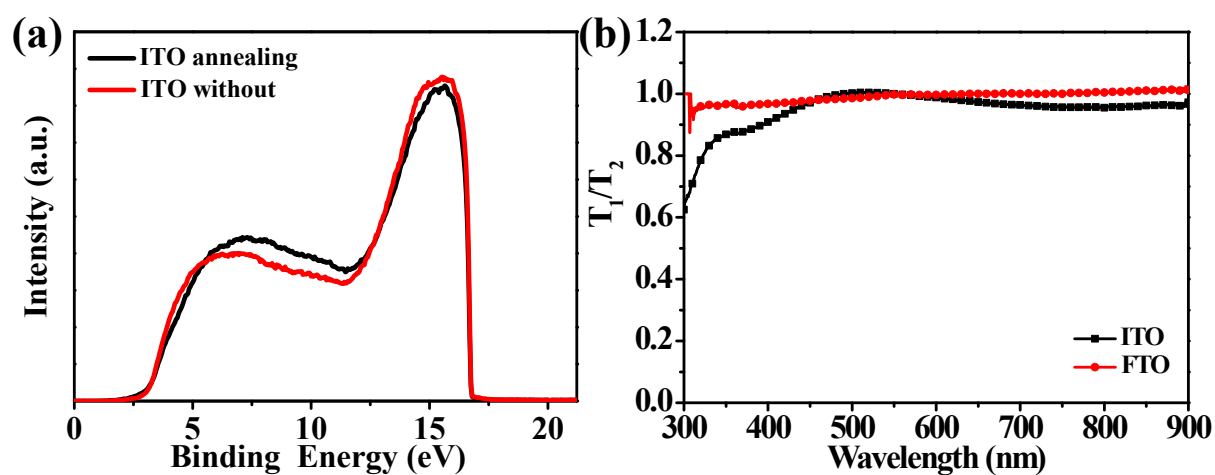


Figure S17 (a) The ultraviolet photoelectron spectra of ITO substrates (with and without annealing). (b) The normalized curve of transparency about ITO and FTO substrates ( $T_1$  with annealing,  $T_2$  without annealing).

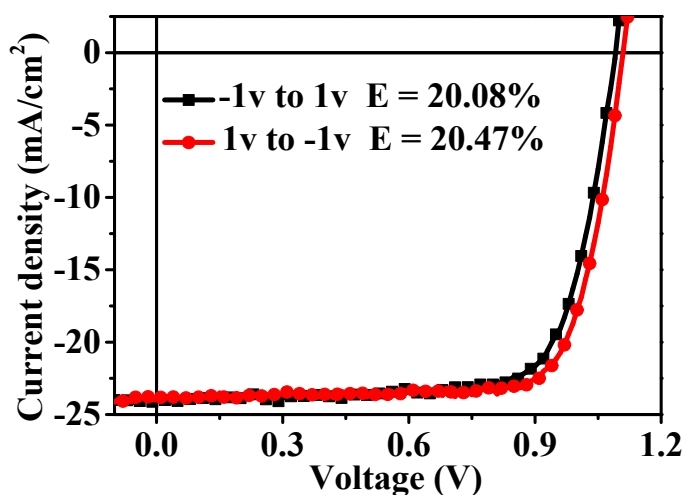


Figure S18 The J-V curves of  $\text{CH}_3\text{NH}_3\text{PbI}_{3-x}\text{Cl}_x$  device with different sweep directions.

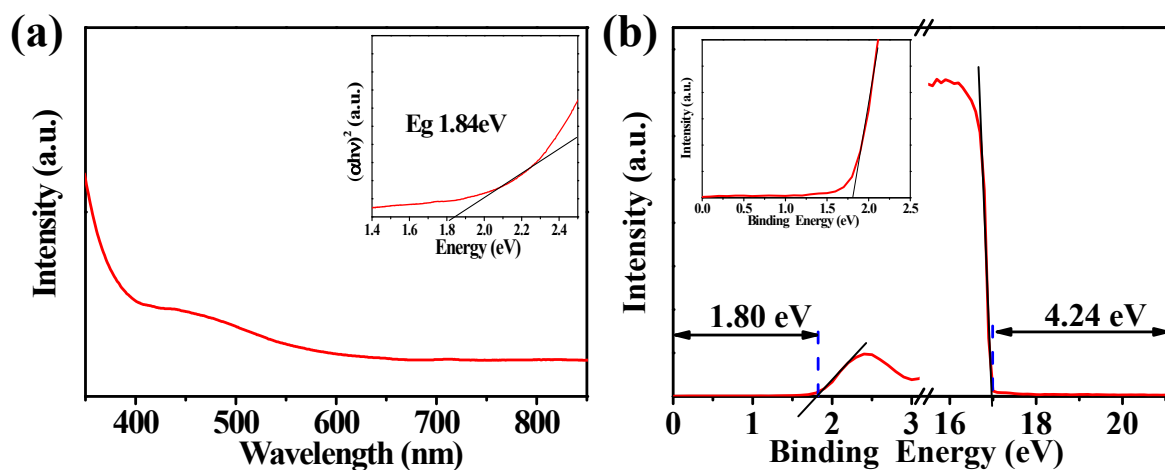


Figure S19 (a) Absorbance spectrum of  $\text{PC}_{61}\text{BM}$  film on ITO substrates, inset shows the corresponding Tauc plot. (b) The ultraviolet photoelectron spectrum of  $\text{PC}_{61}\text{BM}$ , inset zooms in the low binding energy region.

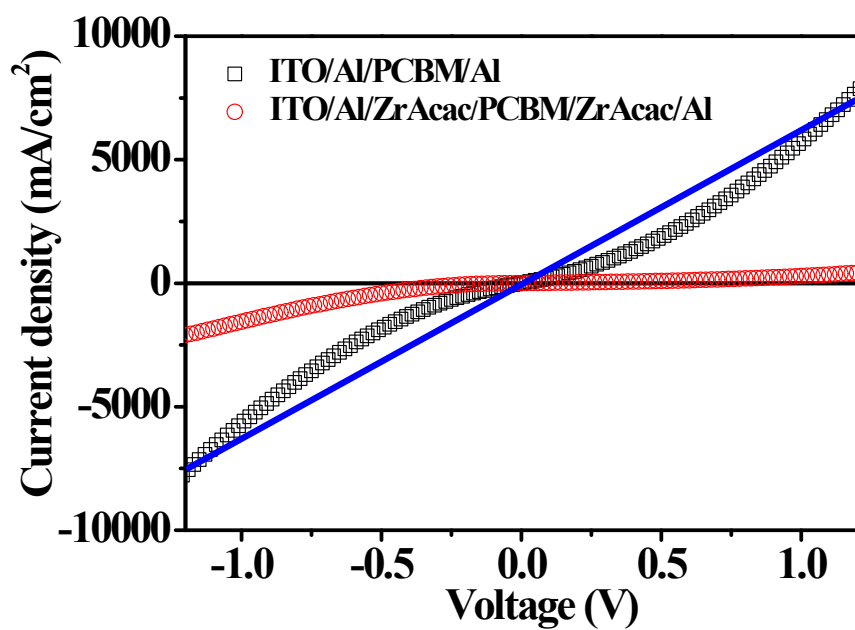


Figure S20 The dark J-V curves of the devices with different structure.

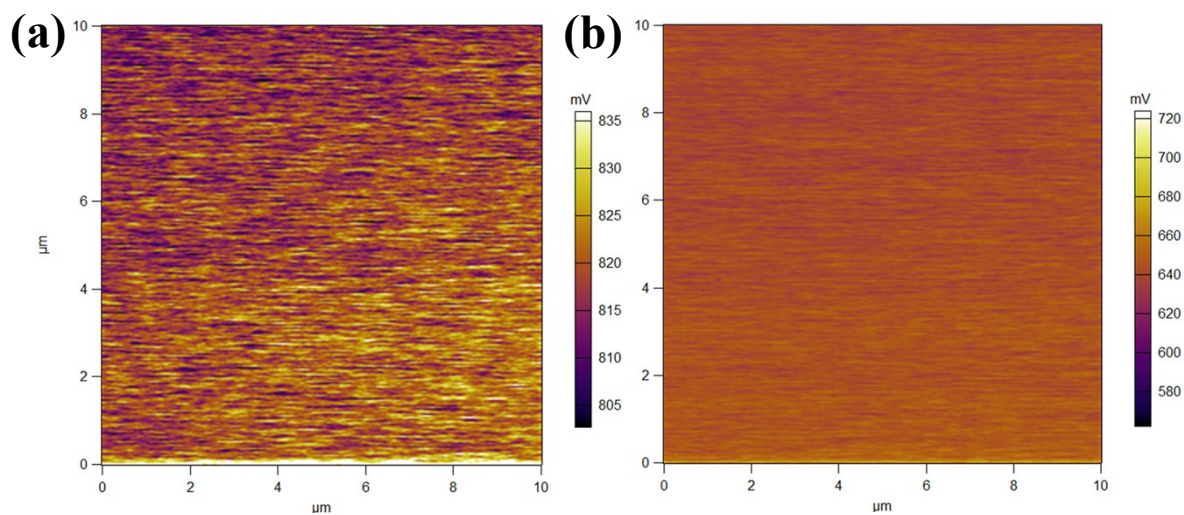


Figure S21 The SKPM images of surface potential for (a) Al coated with ZrAcac (b) Al.

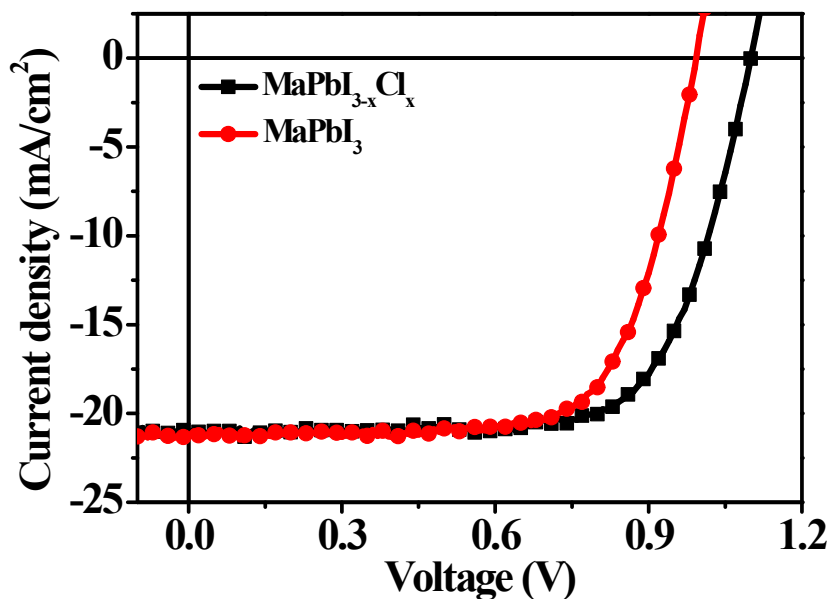


Figure S22 The J-V curves of devices with different active layer under AM 1.5.

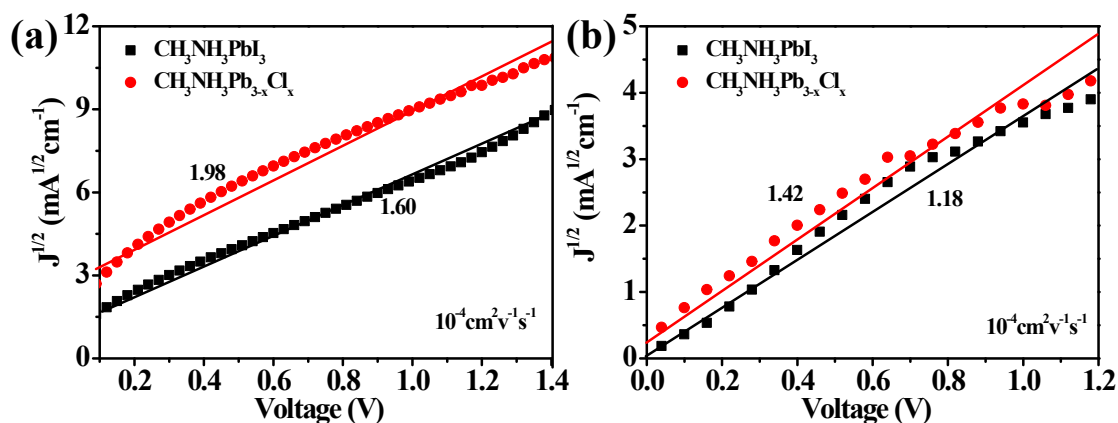


Figure S23 (a)  $J^{1/2}$ -V curves of the hole-only devices with the structure of ITO/NiO<sub>x</sub>+5%Cu/CH<sub>3</sub>NH<sub>3</sub>PbI<sub>3</sub> or CH<sub>3</sub>NH<sub>3</sub>PbI<sub>3-x</sub>Cl<sub>x</sub>/Au. (b)  $J^{1/2}$ -V curves of the electron-only devices with the structure of ITO/Al/ CH<sub>3</sub>NH<sub>3</sub>PbI<sub>3</sub> or CH<sub>3</sub>NH<sub>3</sub>PbI<sub>3-x</sub>Cl<sub>x</sub> /PC<sub>61</sub>BM/ZrAcac/Al. The value in the figure is the corresponding electron or hole mobility.

**Table S1** The  $V_{\text{TFL}}$  and electron trap-states of the corresponding electron-only devices.

	reference	ethanol	2mgml <sup>-1</sup>	4mgml <sup>-1</sup>
$V_{\text{TFL}}$ [V]	1.96	1.66	1.47	1.47
Electron trap-states [10 <sup>16</sup> cm <sup>-3</sup> ]	9.8	8.5	7.5	7.5

**Table S2** The fitting result of impedance spectra for the devices in figure 2f.

Samples	$R_s$ [ $\Omega$ ]	$R_1$ [ $\Omega$ ]	$R_2$ [ $\Omega$ ]
reference	162	1590	100
ethanol	135	340	100
2mgml <sup>-1</sup>	130	170	15
4mgml <sup>-1</sup>	119	1850	1689

**Table S3** The hole mobility of the corresponding hole-only devices.

Hole mobility	0% Cu	5% Cu	20% Cu
10 <sup>-4</sup> cm <sup>2</sup> v <sup>-1</sup> s <sup>-1</sup>	0.52	0.88	0.66

**Table S4** The  $V_{\text{TFL}}$  and hole trap-states of the corresponding hole-only devices.

	0% Cu	5% Cu	20% Cu
$V_{\text{TFL}}$ [V]	0.67	0.6	>1
Hole trap-states [ $10^{16}\text{cm}^{-3}$ ]	3.42	3.06	>5.10

**Table S5** The fitting result of impedance spectra for the devices in figure S16.

Samples	$R_s$ [ $\Omega$ ]	$R_1$ [ $\Omega$ ]	$R_2$ [ $\Omega$ ]
0% Cu	95	430	25
5% Cu	130	170	15
20% Cu	122	276	26

**Table S6** The fitting result of impedance spectra for the devices in figure 5c.

Samples	$R_s$ [ $\Omega$ ]	$R_1$ [ $\Omega$ ]	$R_2$ [ $\Omega$ ]
FTO	29	75	17
ITO	130	170	15

## References

1. H. Yu, F. Wang, F. Xie, W. Li, J. Chen and N. Zhao, *Advanced Functional Materials*, 2014, **24**, 7102–7108.
2. E. Mosconi, A. Amat, M. K. Nazeeruddin, M. Grätzel and F. De Angelis, *The Journal of Physical Chemistry C*, 2013, **117**, 13902-13913.
3. L. Zhu, J. Shi, S. Lv, Y. Yang, X. Xu, Y. Xu, J. Xiao, H. Wu, Y. Luo, D. Li and Q. Meng, *Nano Energy*, 2015, **15**, 540-548.
4. S. Petit, S. Morlens, Z. Yu, D. Luneau, G. Pilet, J.-L. Soubeyroux and P. Odier, *Solid State Sciences*, 2011, **13**, 665-670.